Faraday
Discussions

Accepted Manuscript

Faraday Discussions

Royal Society of Chemistry

ROYAL SOCIETY OF CHEMISTRY

www.rsc.org/faraday_d

Understanding the Processes Governing Performance and Durability of Solid Oxide Electrolysis Cells

Sune Dalgaard Ebbesen,* Xiufu Sun and Mogens Bjerg Mogensen

Operation of Ni-YSZ electrode supported Solid Oxide Cell (SOC) was studied in both fuel cell mode (FC-mode) and electrolysis cell mode (EC-mode) in mixtures of H_2O/H_2, CO_2/CO, $H_2O/H_2O/CO_2/CO$ at 750ºC, 800ºC and 850ºC. Although the
10 SOCs are reversible, the polarisation characterisation show that the kinetics for reduction of H_2O and CO_2 is slower compared to oxidation of H_2 and CO, and that oxidation/reduction in CO_2/CO mixtures is slower than in H_2O/H_2 mixtures. The kinetic differences are partly related to the polarisation heating and the entropy change. Also the diffusion resistance is larger in EC-mode as compared to FC-mode
15 and the low frequency concentration resistance (which is affected by diffusion), is asymmetric around OCV, and is significant higher in EC-mode. Both the increased diffusion resistance and the asymmetric low frequency concentration resistance result in a decreased activity in EC-mode. Changing the porosity of the support structure shows a significant change in both the diffusion resistance and low
20 frequency concentration resistance when applying current, showing that diffusion limitations cannot be neglected for SOCs operated in EC-mode. Also the Ni-YSZ TPB resistance is affected by changing the support porosity, indicating that kinetic investigations under current and even at OCV, and the chase for a general expression for "all" Ni-YSZ electrodes may be pointless.
25 The diffusion limitations through the support and active electrode structure create an increased reducing atmosphere at the interface which may be related to the degradation of the cells.

Introduction

The reversibility of solid oxide cells (SOCs), thus that they can be operated as both a
30 solid oxide fuel cell (SOFC) and a solid oxide electrolysis cell (SOEC), was demonstrated for both H_2O[1-9] and CO_2[1;9-13] in the early 1980'ies. Although the cells are reversible a slightly lower performance and an increased degradation is normally observed in electrolysis cell mode (EC-mode)[14-17], and reactant starvation is generally observed at lower current densities and degrees of conversion in EC-mode
35 as compared to FC-mode. For both H_2O/H_2 and CO_2/CO mixtures a marginally higher activity towards H_2 or CO oxidation i.e. in fuel cell mode(FC-mode) is found in comparison to H_2O or CO_2 reduction (operation in EC-mode)[14;18-23]. Based on a theoretical study, it was suggested that this difference between oxidation and reduction lies in the slower diffusion of H_2O compared to H_2[24]. A recent study have
40 showed that the lower performance in EC-mode may be caused by an increased low frequency concentration resistance in EC-mode as well as a local temperature decrease in EC-mode as compared to FC-mode due to the exothermic nature of the oxidation and endothermic nature of the reduction.[25] It was further speculated that the increased low frequency concentration resistance was caused by diffusion to the

active Ni-YSZ electrode, depleting the reactants at the active Ni-YSZ electrode[25]. Beside the increased diffusion, the lower performance may be related to the increased Ni-YSZ polarisation resistance in dry conditions[26;27].

The performance during CO_2 electrolysis is found to be significantly lower than during H_2O electrolysis at identical conditions[1;14;18;19;27]. Beside the significantly different reaction mechanisms for the two electrolysis reactions[22;27-29], the performance during CO_2 electrolysis may be due to the slower diffusion of CO_2/CO compared to H_2O/H_2[24;30-34], leading to an increased diffusion and low frequency concentration resistance, and a larger Ni-YSZ electrode TPB resistance due to the increasing reducing atmosphere caused by diffusion limitations

A number of possible rate determining steps have been identified for the Ni-YSZ electrode when operating in both FC-mode and EC-mode in mixtures of hydrogen, carbon monoxide, steam, carbon dioxide and methane[22;27-29;35-40] which are very dependent on electrode structure and composition. In general there is a large disagreement regarding understanding of the processes occurring in the SOCs[14] and the apparent activation energy, current-voltage relationship (i-V curve), measured impedance, dependence of the i-V curve on partial pressure of reactants and products, vary hugely.[26;41-51] The partial pressure dependency seems to be related to both the performance of the cell and level of degradation[25] as well as on the electrode micro structure[52-54].

Although no direct evidence has been presented, it is generally believed that SOECs show larger degradation during CO_2 electrolysis (and co-electrolysis of steam and CO_2) as compared to steam electrolysis.[14] Further it is believed that increasing the steam/CO_2 concentration may increase degradation[55;56], and that an increased conversion degree may increase in the degradation rate[57;58]. The observed degradation may further be dependent on both the initial cell performance and micro-structure.[14;59-63]

In this paper we try to correlate some of the differences observed when operating the SOC in either fuel cell or electrolysis cell mode as well as the differences between the reaction rates observed during steam electrolysis and carbon dioxide electrolysis with variations in the cell structure and the degradation of these cells.

Experimental

Solid Oxide Cells

Planar Ni-YSZ supported SOCs of 5×5 cm^2 with an active electrode area of 4×4 cm^2 were used for the experiments. Cells with an LSM-YSZ oxygen electrode (denoted: Ni-YSZ|YSZ|LSM-YSZ cells) and cells with an LSCF-CGO (denoted: Ni-YSZ|YSZ|CGO|LSCF-CGO cells) oxygen electrode were applied for the study.[15;64] The Ni-YSZ support/electrode was nominally the same for all the cells. The cells were supported by a ~300 μm thick porous Ni-YSZ layer[64;65], and have a 10 – 15 μm thick Ni-YSZ cermet electrode; a 10 – 15 μm thick YSZ electrolyte and a 15 – 20 μm thick either strontium-doped lanthanum manganate (LSM-YSZ) or strontium-doped lanthanum ferrite partial substituted with cobalt (LSCF-CGO) composite oxygen electrode. For the cell with the LSCF-CGO oxygen electrode, a CGO barrier layer (5 – 10 μm thick) between the electrolyte and the LSCF-CGO oxygen electrode was applied. Although the Ni-YSZ support/electrode were nominally the same for all the cells, different processing parameters resulted in a support structure porosity of 34% for the Ni-YSZ|YSZ|LSM-YSZ cells whereas a lower porosity of

28% for the Ni-YSZ|YSZ|CGO|LSCF-CGO cells.

For characterising the cell as well as durability testing, a test house as shown in Figure 1 and described in details elsewhere[66] was used. A total of 15 cells were tested for the experiments shown in the present study. Reduction of the nickel oxide
5 in the Ni-YSZ electrode was performed in hydrogen at 1000ºC for 13 of the cells, whereas the remaining two cells (used to compare the degradation rate for CO_2 and steam electrolysis) were reduced at 850ºC. The experiments shown in this study have been reproduced on several Ni-YSZ based SOCs and all initial i-V curves and impedance spectra were reproducible. On the other hand, when performing
10 durability studies at high current (at or above -1A/cm^2) structural degradation occurs, which makes the degradation rate is difficult to reproduce.[67]

The DC characterisation of the cells was performed by recording polarisation curves (i-V curves) in both electrolysis and fuel cell mode by varying the current. AC characterisation was performed by Electrochemical Impedance Spectroscopy (EIS)
15 using an external shunt and a Solartron 1255B or 1260 frequency analyser at frequencies from 82 kHz to 0.08 Hz (when applying 6 points pr. decade) or 96 kHz to 0.096 Hz (when applying 12 points pr. decade) with an amplitude of 60 mA. The impedance data were corrected using the short-circuit impedance response of the test set-up.
20 We have previously shown that the gas purity has a significant effect on the degradation of the SOCs operated in both EC and FC-mode.[66;68;69] In order to eliminate impurity related degradation, the inlet gases to the Ni-YSZ electrode compartment were cleaned by flowing the inlet gasses (except oxygen) over porous Ni-YSZ particles at 700 - 725ºC in order to catch/adsorb all impurities that would
25 otherwise be adsorbed on the active Ni-YSZ TPBs in the SOC.[70;71]

Effect of porosity in the Ni-YSZ support and electrode

Ni-YSZ|YSZ|LSM-YSZ cells with different Ni-YSZ cermet porosity were produced by sintering identical half cells (Ni-YSZ support, Ni-YSZ active electrode and electrolyte) at temperatures ranging from 1255 to 1335 ºC. Several cells are shown
30 in the present study, with porosity varying from 23% to 31% in the support structure and 13% to 18% in the active Ni-YSZ electrode[72;73]. The structural parameters for each cell are given in the text. The stated porosity is based on analysis of SEM images on reference cells and should be taken as indications only. These experiments are not used to give any specific values, but are used to show specific
35 trends related to the porosity.

Characterisation

Performance as a function of gas composition (pH$_2$, pH$_2$O, pCO, and pCO$_2$)

After an initial AC and DC characterisation, additional EIS was recorded while varying pH$_2$, pH$_2$O, pCO, and pCO$_2$. Varying the hydrogen concentration in the
40 H$_2$O/H$_2$ mixture was performed by keeping the steam concentration fixed at 15% and varying the hydrogen concentration from 85 % down to 35 % by exchange with argon. When varying the steam concentration, both the steam and hydrogen concentration was varied since the first experiment with changing the hydrogen concentration showed that the hydrogen dependency is negligible (see result and
45 discussion section). The steam concentration was varied from 15% to 85% with hydrogen as the remaining gas.

Varying the carbon monoxide and carbon dioxide concentration in the CO_2/CO mixture was examined at a narrower interval in order to avoid solid carbon

formation in the Ni-YSZ electrode (and the Ni-YSZ powder used for cleaning the inlet gases, operated at 700 - 725ºC). Varying the CO concentration in the CO_2/CO mixture was performed by keeping the CO_2 concentration fixed at 30% and varying the hydrogen concentration from 65 % down to 15 % by exchange with argon.

5 Varying the CO_2 concentration in the CO_2/CO mixture was performed by keeping the CO concentration fixed at 30% and varying the CO_2 concentration from 70 % down to 20 % by exchange with argon. When varying both the CO and CO_2 concentration (pCO+pCO$_2$=1) CO_2 concentration was varied from 30% to 80% with CO as the remaining gas.

10 **Performance as a function of current density**

The performance as a function of applied current was examined in both EC-mode and FC-mode. Electrochemical Impedance Spectra (EIS) were recorded in 50% H_2O/50% H_2 or 50% CO_2/50% CO at current densities varying from either +0.5 or +0.7 A/cm^2 (FC-mode) to either -0.5 or -0.7 A/cm^2 with steps of 0.1 A/cm^2 (EC-

15 mode). After setting the current, the cell was left at the applied current density for 15 minutes before the impedance measurement was initiated.

Flow variations under current

The performance under current at varying flowrates was examined by performing EIS measurement under current while keeping the average pH_2O constant at 0.50,

20 while varying the current density and flowrate according to .

Table 1. Conditions for flow variations under current.

Flow rate (L/h)		Fuel cell mode			Electrolysis cell mode		
Flow rate (L/h)	1/ Flow rate (L/h^{-1})	Current density (A/cm^2)	Inlet gas composition (pH$_2$O)	Average gas composition (pH$_2$O)	Current density (A/cm^2)	Inlet gas composition (pH$_2$O)	Average gas composition (pH$_2$O)
15.0	0.067	0.30	0.43	0.5	- 0.30	0.57	0.5
17.5	0.057	0.35	0.43	0.5	- 0.35	0.57	0.5
20.0	0.050	0.40	0.43	0.5	- 0.40	0.57	0.5
22.5	0.044	0.45	0.43	0.5	- 0.45	0.57	0.5
25.0	0.040	0.50	0.43	0.5	- 0.50	0.57	0.5

Performance as a function of temperature

The performance as a function of temperature was investigated in steam/hydrogen mixtures by recording impedance spectra with a constant pH_2O of 0.50 at

25 temperatures ranging from 850 to 900ºC.

Durability testing

The durability of the Ni-YSZ based SOCs was examined for H_2O and CO_2 electrolysis and co-electrolysis of H_2O and CO_2. All cells were operated at with oxygen flown to the oxygen electrode, and a current density of -1.0 A/cm^2. Both the

30 flowrate and gas composition to the Ni-YSZ electrode was varied.

One series of experiments to investigate the temperature dependency on the degradation was carried out for six cells (three Ni-YSZ|YSZ|LSM-YSZ cells, and three Ni-YSZ|YSZ|CGO|LSCF-CGO cells), operated at 750ºC, 800ºC or at 850ºC. Three experiments were performed on the Ni-YSZ|YSZ|LSM-YSZ cells, and Ni-

35 YSZ|YSZ|CGO|LSCF-CGO cells. For these six experiments the durability was examined during co-electrolysis, with 45% H_2O/ 45% CO_2/ 10% H_2 flown to the Ni-

YSZ electrode. The tests were carried out with a H_2O+CO_2 conversion at 60%. Additionally, one experiment was carried out at 800ºC with a H_2O+CO_2 conversion of 30% by increasing the flowrate to the Ni-YSZ electrode (keeping the current density of -1.0 A/cm^2). The effect of reactant conversion was further examined

5 during steam electrolysis (to avoid carbon deposition at high conversion) in 90% H_2O/ 10% H_2 at 800°C by changing the flowrate to the Ni-YSZ electrode (keeping the current density of -1.0 A/cm^2) with an initial H_2O conversion degree of 30% and subsequently increased by steps of 10% conversion. Finally two tests were conducted in order to examine the degradation rate of steam electrolysis (90%

10 H_2O/10% H_2) and CO_2 electrolysis (90% CO_2/10% CO) at 800°C.
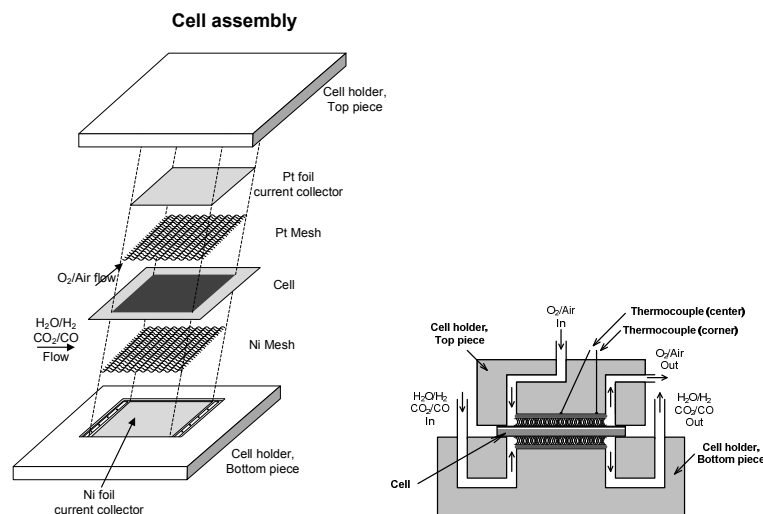
Figure 1. Cell assemblies in a cross-flow pattern. A: Exploded view of the cell assembly, and B: Side view of the cell assembly showing the gas flow directions and the placement of thermocouples, it has to be noticed that the flow directions shown in figure B is in co-flow pattern, whereas the

15 actuarial flow during the experiments were cross-flow.

Modelling the current and overpotential along the cell

The distribution of the current and overvoltage along the cell in the flow direction was modelled in order to estimate the effect of both support structure and conversion degree on the overvoltage at the Ni-YSZ electrode TPB. The modelling was

20 performed for steam electrolysis only in order to simplify the calculations. For the modelling, the cell was divided into 16 slabs of 1 cm^2 (length of 0.25 cm) along the steam flow direction. Negligible in-plane voltage along the cell was assumed, thus a constant cell voltage along the cell applies. The overpotential cell voltage in each slab along the cell was calculated as following:

25
$$U_{Slab1} = OCV_{Slab1} + \eta_{Slab1} \qquad (1)$$

With the overpotential calculated as:

$$\eta_{Slab1} = R_{Slab1} \cdot i_{Slab1} \qquad (2)$$

The resistance of each slab was calculated by adding all resistances for the individual processes in the cell:

$$R_{Slab1} = R_{Serial,Slab1} + R_{Ox,Slab1} + R_{Ni-YSZ,Slab1} + R_{Diffusion,Slab1} + R_{Conversion,Slab1} \qquad (3)$$

A breakdown of the cell contributions (see Table 3) are used for the serial resistance and the oxygen electrode resistance. The conversion and diffusion resistance was calculated according to the equations described below.

5 *Diffusion resistance*

The diffusion resistance $(R_{Diffusion})$ is related to the change in Nernst potential due to gas diffusion limitations within the porous Ni-YSZ support/electrode. In H_2O/H_2 mixtures $R_{Diffusion}$ can be calculated as:[74]

$$R_{Diffusion} = \frac{\eta_D}{i} = \left(\frac{R \cdot T}{2 \cdot F}\right)^2 \cdot \frac{l}{P \cdot D_{eff}} \cdot \left(\frac{1}{x_{i,H_2O}} + \frac{1}{x_{i,H_2}}\right) \qquad (4)$$

10 Where η_D is the diffusion overpotential, P is the pressure, D_{eff} the effective diffusion coefficient, l is the diffusion length (support thickness), i is the current, R is the gas constant, F is Faradays constant, T is the temperature in Kelvin, x_{i,H_2O} and x_{i,H_2} are the inlet mole fractions of steam and hydrogen. The diffusion resistance in CO_2/CO mixtures is calculated in a similar manner. For diffusion in porous structures, a 15 correlation for the average percolating porosity in the diffusion direction must be made, and in pores smaller than a few microns $(Kn > 10, Kn = {}^{Diffusion\ length}/_{Pore\ Diameter})$ Knudsen diffusion dominates. The Knudsen diffusion coefficient (D_{Kn}) can be calculated as:

$$D_{Kn} = \frac{d_p}{3} \cdot \sqrt{\frac{8 \cdot R \cdot T}{\pi \cdot M}} \qquad (5)$$

20 Where d_p is the pore diameter, M is molar weight of the gases. T h is the temperature in Kelvin. Based on the Knudsen diffusion, the effective diffusion can be calculated as:

$$D_{Kn,eff} = \frac{\varepsilon}{\tau} \cdot D_{Kn} \qquad (6)$$

Where ε is the porosity and τ is the tortuosity. The actual diffusion length through 25 the porous structure is extremely difficult to estimate, and the tortuosity factor describes that the diffusion path through the porous structure is longer than a direct path (electrode/support thickness). Microstructural studies (using e.g. Focused Ion Beam Scanning Electron Microscopes) of fuel electrode supported cells provide evidence that the tortuosity for typical fuel electrode supported SOCs with a porosity 30 around 30% is $1 - 3$.[75-79] In the modelling a tortuosity factor of 1 is used and changes is made in porosity only (Figure 13). Later, an analysis of the actual/experimental determined relation between porosity and tortuosity is made in the discussion.

Conversion resistance

35 The conversion resistance $(R_{Conversion})$ is based on the change in Nernst potential due to conversion and is therefore related to the gas composition. Assuming a continuously stirred tank reactor (CSTR) the impedance caused by gas conversion in $H_2O - H_2$ mixtures at the Ni/YSZ electrode can be expressed as:[80]

$$R_{Conversion} = \frac{\eta_C}{i} = \frac{R \cdot T}{4 \cdot F^2 \cdot J_i} \cdot \left(\frac{1}{x_{i,H_2O}} + \frac{1}{x_{i,H_2}}\right) \qquad (7)$$

40 where η_C is the conversion overpotential, J_i is the inlet area specific flow rate $(mol/m^2\ s)$. i, R, F, T, x_{i,H_2O} and x_{i,H_2} have the same meaning as described above.

The conversion resistance in CO_2/CO and $H_2O/CO_2/H_2/CO$ mixtures may be calculated in a similar manner. Assuming a plug-flow reactor (PFR), the impedance caused by gas conversion is half of the impedance when assuming a continuously stirred tank reactor (CSTR).[81] It has been well proven that the conversion resistance can be calculated as stated in equation 7 at OCV[80], which will also be shown in the present article, whereas under current, this has not been fully investigated[25], and is a part of the present article. Thus at OCV, the conversion resistance is denoted conversion resistance, whereas under current, the changes in Nernst potential due to the changes in concentrations during the AC perturbations caused by the impedance measurements will be denoted "low frequency concentration resistance".

Ni-YSZ TPB resistance

The Ni-YSZ resistance in H_2O/H_2 mixtures can be calculated based on the pH_2O dependency as shown in *Figure 2*. The R_{Ni-TPB} follows a power law dependency on the steam and hydrogen concentration ($pH_2{}^a \cdot pH_2O^b$) where the dependency of H_2 is negligible[25] and the exponent for pH_2O is between -0.30 and -0.32[25].
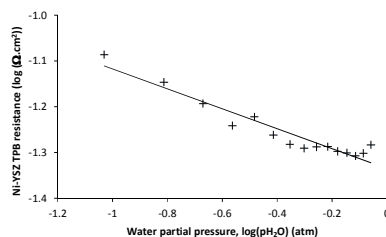
Figure 2. Dependency of Ni-YSZ resistance on the steam concentration.

The current distribution along the cell was calculated by minimizing the error between the calculated cell voltage (according to equation 1) and the actual constant cell voltage by non-linear least-square. The output of the modelling gives the distribution of current along the cell as well as the overpotential of each of the processes occurring in the cell.

Break down of the impedance by fitting to an equivalent circuit model

Cells with an LSM-YSZ oxygen electrode

To break down the impedance contributions from each of the two electrodes, the impedance spectra were fitted to an equivalent circuit model consisting of an inductance, a ohmic resistance (serial resistance R_S), and five constant phase elements (CPE) in parallel - as previously described for this type of Ni-YSZ based SOCs[50]. When characterising the cells with 25% H_2O – 75% H_2 supplied to the Ni-YSZ electrode and air to the LSM-YSZ electrode the five circuits represent a high frequency LSM-YSZ electrode arc[1] ($R_{LSM – High}$), a contribution from the TPB reaction in the Ni-YSZ electrode (R_{TPB}), a low frequency LSM-YSZ electrode TPB arc ($R_{LSM – Low}$), a diffusion arc ($R_{Diffusion}$) and a gas conversion arc ($R_{Conversion}$). $R_{Diffusion}$ and $R_{Conversion}$ originate from the Ni-YSZ electrode. The resistances and frequencies for each of the five circuits when characterising the SOCs produced at DTU Energy with 25% H_2O – 75% H_2 supplied to the Ni-YSZ and air supplied to the LSM-YSZ electrode at 850ºC are listed in Table 2.[50]

Cells with an LSCF-CGO oxygen electrode

---

[1] For the Ni-YSZ|YSZ|LSM-YSZ cells, the high frequency arc corresponds to the O^{2-} transport through the structure of LSM-YSZ electrode which for the Ni-YSZ|YSZ|CGO|LSCF-CGO cells is normally related to the Ni-YSZ electrode. The high frequency arc may therefore be related to the entire O^{2-} transport in the composite electrodes and thus not only in a single electrode.

Also for the cells with an LSCF-CGO oxygen electrode, the impedance contributions were broken down to the contributions from each of the two electrodes, by fitting the impedance spectra to an equivalent circuit model. For the cells with an LSCF-CGO oxygen electrode, the equivalent circuit model consisted of an inductance, a ohmic resistance (serial resistance R_S), and four constant phase elements (CPE). One for the oxygen ion transfer ($R_{O2trans}$, comparable to the $R_{LSM – High}$), one for the TPB reaction in the Ni-YSZ electrode (R_{TPB}), a diffusion arc ($R_{Diffusion}$) and a gas conversion arc ($R_{Conversion}$) similar to the cells with an LSM-YSZ oxygen electrode. In contrast to the cells with an LSM-YSZ oxygen electrode, the contribution for the TPB reaction in the LSCF-CGO oxygen electrode was fitted with a Gerischer element (G).

The resistances and characteristic frequencies listed in Table 2 can only be used as a guideline because variation in performance between the produced cells occur, and since other resistances and frequencies will certainly be observed when changing the gas compositions (see Table 3), i.e. steam partial pressure to the Ni-YSZ electrode and oxygen partial pressure to the LSM-YSZ electrode[50;82]. An initial fit of the spectrum recorded at OCV was obtained by keeping the exponent of the constant phase elements constant[50] and applying the published values for the resistance of each circuit as a starting point. For the subsequent fitting routines a free fit of the resistances and characteristic frequency of the respective processes was performed. Subsequently, the spectra when changing the operation conditions (current and gas composition) were fitted. We are aware that the description of the break-down has been much improved recently[83], but the available break down data to be used here were obtained as described.

Table 2. Break down of the polarisation resistances for the SOCs produced at DTU Energy (former Risø DTU) SOCs when characterised in 25% H_2O – 75% H_2 at the Ni-YSZ electrode and air at the LSM-YSZ electrode at 850ºC. Activation energies are summarised based on literature.

Process	Resistance ($\Omega \cdot cm^2$)	Characteristic frequency (Hz)	Activation energy (eV)
R_s	$0.03 – 0.13$[50]	—	$0.7 – 0.9$[50;84-86]
LSM_{Hi}	$0.05 – 0.07$[50]	50000[50]	1.0[50;86;87]
Ni-YSZ TPB	$0.05 – 0.08$[50]	8000[50]	$0.8 – 1.1$[46;50]
LSCF-CGO		$100 - 200$[88]	1.4[88]
LSM_{Low}	$0.03 – 0.06$[50]	1100[50]	$1.4 – 2.0$[50;53;86;87;89]
Diffusion	$0.02 – 0.03$[50]	20[50]	—
Conversion	~ 0.06[50]	3[50]	—

Results

Performance as a function of current density

Figure *3* shows sets of two i-V curves measured in FC-mode and EC-mode at 850ºC with 50% H_2O/50% H_2 or 50% CO_2/50% CO mixtures supplied to the Ni-YSZ electrode while pure oxygen was supplied to the LSM-YSZ electrode. From the i-V characteristic shown in Figure 3 it is observed that no discontinuity occurs in the shift from FC-mode to EC-mode, although the slopes (Area Specific cell Resistance, ASR) were higher in EC-mode compared to FC-mode. In FC-mode, the ASR was $0.20~\Omega.cm^2$ in agreement with previous measurements for identical SOCs[90]. The ASR in EC-mode was $0.21~\Omega.cm^2$, showing a marginal higher activity towards

oxidation of H_2 than reduction of H_2O for the Ni-YSZ electrode as reported previously [20;21]. The ASR for oxidation of CO, when supplying 50% CO_2/50% CO to the Ni-YSZ electrode was 0.24 and an ASR of 0.25 $\Omega.cm^2$ were found for reduction of CO_2. The cells thereby showed lower activity for CO_2 reduction than for CO
5 oxidation as previously observed, and lower activity for CO oxidation compared to H_2 oxidation in agreement with literature[91]. Finally the cells also showed slower kinetics for CO_2 reduction than for H_2O reduction as have also previously been reported.

Figure *3* also shows the temperature evolution during the measurement of the i-V
10 curves. Also the production/consumption of heat showed differences when comparing operation in FC-mode and EC-mode, where heat is produced in FC-mode, and consumed in EC-mode, and that production/consumption is larger in the CO_2/CO mixture compared to the H_2O/H_2 mixture.
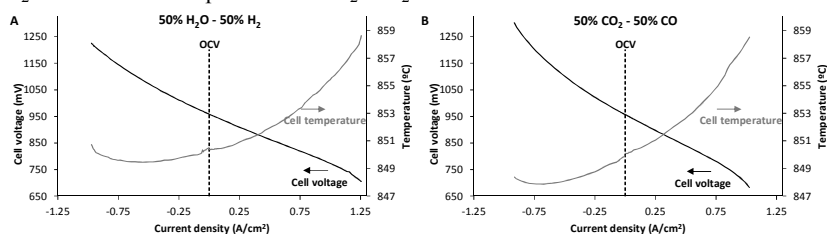
15 Figure 3. DC characterisation at 850ºC, A: in 50% H_2O/50% H_2, B: in 50% CO_2/50% CO. The measured cell temperature while performing the DC characterisation is indicated.

Electrochemical impedance spectra measured at current densities varying from -0.5 A/cm^2 (operation in EC-mode) to +0.5 A/cm^2 (operation in FC-mode) while supplying 50% H_2O/50% H_2 to the Ni-YSZ electrode are shown in Figure 4C and D.
20 The measured cell voltage and cell temperature while recording the impedance spectra are shown in Figure 4A. Similar sets of impedance spectra, cell voltage and cell temperature while supplying 50% CO_2/50% CO to the Ni-YSZ electrode are shown in Figure 4B, D and F.

The cell temperature and cell voltage follows the same pattern as in Figure *3*. The
25 impedance spectra in Figure 4C – Figure 4F shows that during reduction (EC-mode) both the ohmic and polarisation resistance increases with increasing electrolysis current density, whereas during oxidation (FC-mode) both the ohmic and polarisation resistance decreases with increasing positive current density. The evolution in impedance is further analysed by a breakdown of the resistance of the
30 individual electrode processes (Figure 5).
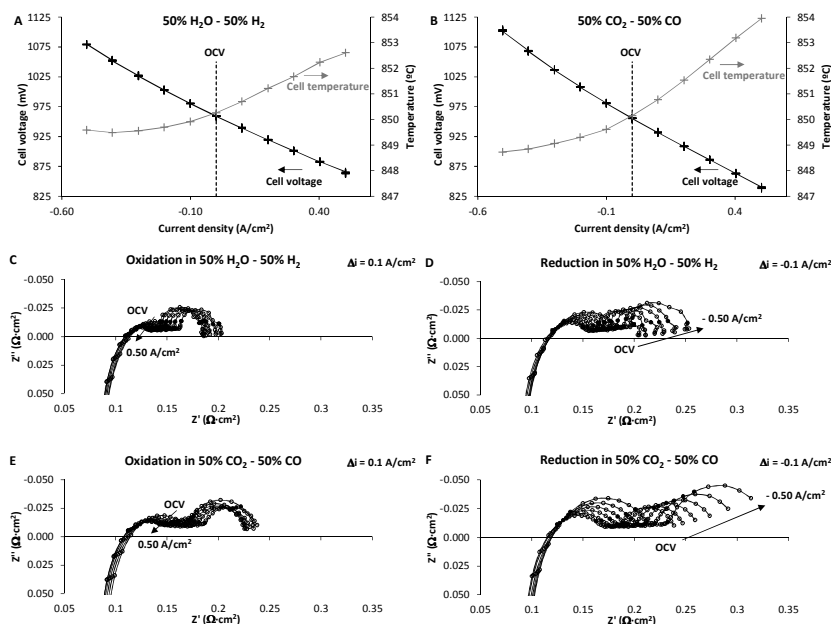
Figure 4. DC (A, B) and AC (C, D, E, F) characterisation at 850°C in mixtures of 50% H_2O/50% H_2
(A, C and E) and 50% CO_2/50% CO (B, D and F). The points on the curves for DC characterisation
(A and B) indicate the measuring points for the AC characterisation. AC characterisation was
performed at OCV and during oxidation at current densities up to +0.5 A/cm^2 (C and E) and during
reduction at current densities to -0.5 A/cm^2 (D and F).

To establish the characteristic frequencies for each of the processes contributing to
the total polarisation of the cell, DRT analysis for the initial impedance spectra
while varying pH_2O, pH_2, pCO_2, and pCO at the Ni-YSZ and pO_2 at the oxygen
electrode was performed at 850°C. As anticipated a change in resistance was
observed at three distinctive frequency regions (~5 Hz, 100 – 110 Hz, and 7000 –
7500 Hz) for the Ni-YSZ electrode when changing the H_2O/H_2 ratio. These
frequencies and are assigned to the resistance caused by gas conversion (~5 Hz), gas
diffusion (100 – 110 Hz) and resistance at the TPB (7000 – 7500 Hz). Similar
characteristic frequencies are observed when performing the CO_2/CO gas-shift (~2
Hz, 55 – 60 Hz, and 6500 – 7000 Hz) and are also assigned to the resistance caused
by gas conversion (~2 Hz), gas diffusion (55 – 60 Hz) and resistance at the TPB
(6500 – 7000 Hz). For the pO_2 shift, also two characteristic frequencies are observed
(~5 Hz, and 1900 – 2000 Hz). The change observed at ~5Hz has been assigned to gas
conversion at the Ni-YSZ electrode and may be caused by a gas-leak, whereas the
change observed at 1900 – 2000 Hz is characteristic for the LSM-YSZ electrode.
Further, one characteristic frequency (50000 Hz[50]) was reported for the LSM-YSZ
electrode, this response show only a small or no pO_2 dependence and is therefore not
observed during the pO_2 shift. The characteristic frequencies are summarised in
Table 3 and used as a basis for fitting the changes in impedance observed when
applying current.

Table 3. Break down of the polarisation resistances for the SOCs produced at DTU Energy (former Risø DTU) when characterised in 25% H_2O – 75% H_2 at the Ni-YSZ electrode and air at the LSM-YSZ electrode at 850ºC [50].

Circuit		H_2O/H_2		CO_2/CO	
		Resistance ($\Omega \cdot cm^2$)	Characteristic frequency (Hz)	Resistance ($\Omega \cdot cm^2$)	Characteristic frequency (Hz)
	Ohmic resistance	0.068	—	0.068	—
1	LSM_{High}	0.039	53000	0.040	53000
2	Ni-YSZ TPB	0.037	7500	0.051	7000
3	LSM_{Low}	0.012	1900	0.012	1900
4	Diffusion	0.009	110	0.013	60
5	Conversion	0.037	$3.9^{20\%} - 4.0^{50\%} (3.4^{70\%})$	0.056	$1.5^{50\%} - 2.6^{70\%}$
	Total	0.202		0.240	

Based on the characteristic frequencies (Table 3) polarisation resistance of the cell was broken down to the contribution for each of the processes occurring in the cell while applying current in both EC-mode and FC-mode. As can be seen from Figure 5, the total resistance (ohmic and polarisation) is higher in EC-mode as compared to FC-mode as previous observed[18-22]. The total resistance increases with increasing negative current density in EC-mode, whereas the total resistance decreases with increasing positive current density in FC-mode. The ohmic resistance follows the change in temperature; the ohmic resistance increases in EC-mode, whereas the ohmic resistance decreases in FC-mode.

From the breakdown of the individual polarisation resistances, it can be seen that the resistance for Ni-YSZ TPB, LSM_{low} and LSM_{hi} increases in EC-mode, whereas they decrease in FC-mode similar to the change in ohmic resistance.
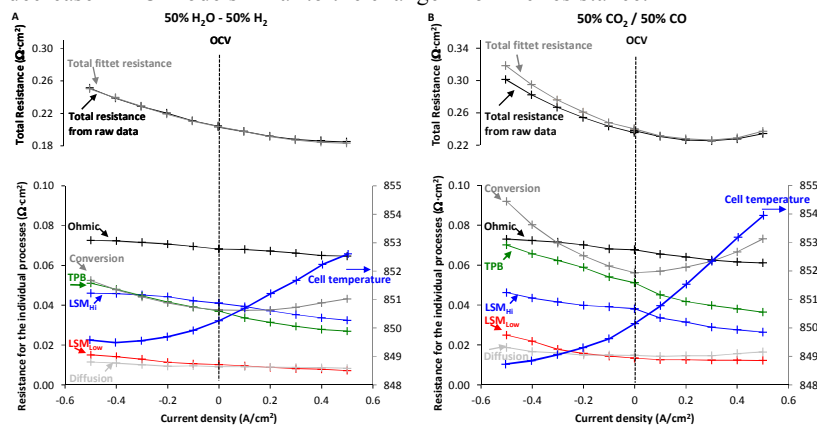
Figure 5. Measured ohmic resistance and break down of the polarisation resistances for the electrochemical impedance spectra shown in Figure 4 during oxidation and reduction at 850ºC in A: 50% H_2O/50% H_2 and B: 50% CO_2/50% CO.

In the present paper, we focus on the diffusion and conversion resistances, and the relation between those. In the H_2O/H_2 mixture, hardly any change in the diffusion resistance is observed when applying current (Figure 6). On the other hand, in the CO_2/CO mixture, the diffusion resistance decreases when applying current in EC-mode, whereas it increases when applying current in FC-mode. The bold lines in

Figure 6A represents the theoretical diffusion resistances. Finally, the low frequency concentration resistance increases with both increasing positive and negative current densities according to the changes in gas composition. The bold lines in Figure 6B represent the theoretical conversion resistances based on the CSTR or a PFR model.
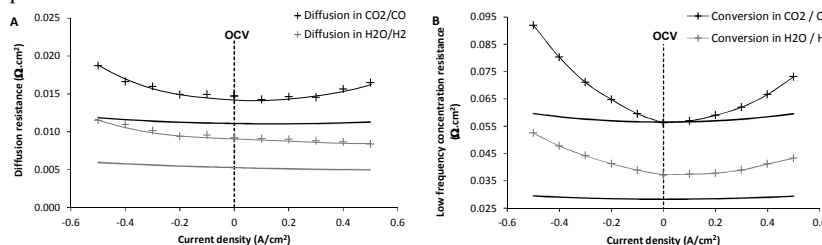
Figure 6. A: Measured (fitted) and calculated theoretical diffusion resistances for the cell as a function of current density in 50% H_2O/ 50% H_2 and 50% CO_2/50% CO. The solid lines are the theoretical diffusion resistances. B: Measured (fitted) and calculated theoretical conversion resistances for the cell as a function of current density in 50% H_2O/ 50% H_2 and 50% CO_2/50% CO. The solid lines are the theoretical conversion resistance for H_2O/ H_2 mixtures based on a CSTR and a PFR model respectively.

The main difference in H_2O/H_2 mixtures and CO_2/CO mixtures lies in the higher diffusion, and the higher low frequency concentration resistance. The higher diffusion resistance in CO_2/CO mixtures implies that the actual gas composition at the active electrode is different from the bulk gas composition. We have previously speculated the increased low frequency concentration resistance was caused by diffusion to the active Ni-YSZ electrode, depleting the reactants at the active Ni-YSZ electrode, and that the low frequency concentration resistance reflects the gas composition at the active Ni-YSZ electrode[25]. In order to verify these hypotheses, the performance as a function of current density was examined for cells with different porosity.

Dependency on Ni-YSZ support structure porosity

Electrochemical impedance spectra measured at OCV for three different cells with a support structure porosity of either 25%, 27% or 31% while supplying 50% H_2O/50% H_2 to the Ni-YSZ electrode and pure oxygen to the oxygen electrode are shown in Figure 7A.

The most distinct difference between the three spectra is in the Ni-YSZ TPB resistance which increases with decreasing porosity. Also, a trained eye can see that significant diffusion resistances are visible, and that the diffusion resistance increase with decreasing porosity. Further, also the conversion resistance increases with decreasing porosity. A visualisation of the Ni-YSZ TPB resistance and diffusion resistance at varying porosity is shown in Figure 7B. The conversion resistance was measured on a large number of cells; including those shown in Figure 7A and the measured conversion resistance at varying porosity is shown in Figure 7C. All measured conversion resistances shown in Figure 7C fall within the values predicted by the CSTR (0.057 $\Omega.cm^2$) or PFR (0.028 $\Omega.cm^2$) models.
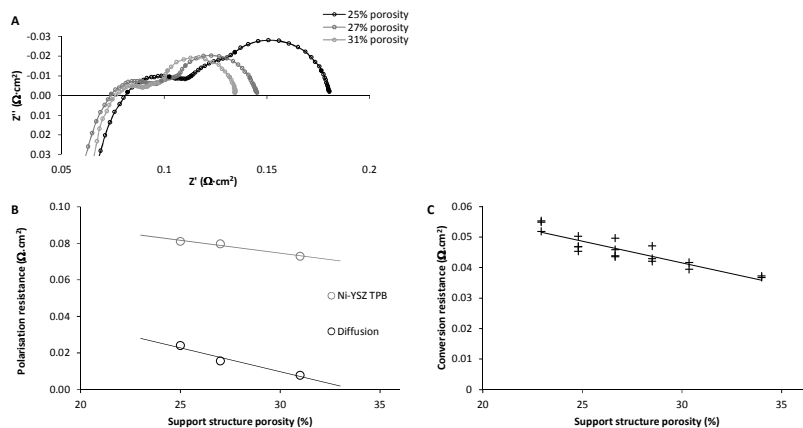
Figure 7. A: Nyquist plot of the AC characterisation at OCV for cells with varying porosity (25, 27 and 31%) when characterised at 850ºC in 50% H_2O/50% H_2. B: Ni-YSZ TPB resistance and
5 resistance caused due to diffusion for the three cells shown in figure A, and C: Resistance caused by gas conversion for a large collection of cells with varying porosity when characterised at 850ºC in 50% H_2O/50% H_2.

The resistance caused by diffusion through the porous support structure depend on the support porosity as shown in Figure 7. The impedance breakdown of the
10 diffusion (Figure 8A) and low frequency concentration resistance (Figure 8B) under current as a function of support structure is shown in Figure 8. Clearly the diffusion resistance increases when applying current in EC-mode. On the other hand, in FC-mode, the diffusion resistance remain close to unchanged. The resistance for the low frequency concentration arc show a similar asymmetric behaviour (similar to the
15 results shown in Figure 5 and Figure 6B) with a large increase in EC-mode and much smaller increase in FC-mode. Further, the resistance for the low frequency concentration arc show a clear dependency on the support structure, with an increased resistance at low porosity and an increased asymmetry with lowering the support structure porosity. This is a clear indication that a significant part of this low
20 frequency resistance originates from diffusion limitations, and may be related to the gas composition at the active Ni-YSZ electrode[25].
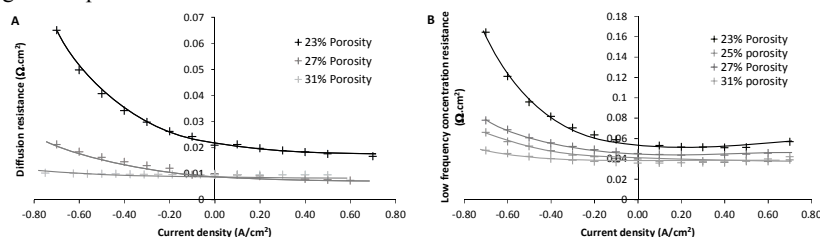
Figure 8. A: Measured (fitted) diffusion and B: low frequency concentration resistance at 850ºC under current (in 50% H_2O/50% H_2).

25 The resistance for the low frequency concentration arc under current in both FC-mode and electrolysis cell mode at varying flowrates are shown in Figure 8A for the cell with 25% porosity in the support structure. The resistance for the low frequency concentration arc under current in EC- mode for cells with varying porosity is shown in Figure 8B. The experiments were conducted such that the average steam

composition was kept constant by changing, beside the flowrate, also the current density, and steam/hydrogen ratio (when shifting between FC-mode end EC-mode) according to the conditions stated in **Error! Reference source not found.**. The bold ines in Figure 8A represent the theoretical conversion resistances based on the

5 CSTR or a PFR model.

For the cell with 25% porosity in the support structure (Figure 8A) a higher low frequency concentration resistance is measured in EC-mode as compared to FC-mode at the same current density and flowrate. Further, a linear dependency between the low frequency concentration resistance and the inverse flowrate is observed in

10 FC-mode, whereas in EC-mode, this relation is only observed at low flowrates and low current density (a similar trend is observed for the remaining cells, not shown). For the cell with a high porosity in the support structure, a dependency close to a linear is also observed in EC-mode (Figure 8B), while decreasing the porosity, and the deviation at high current increases.

15
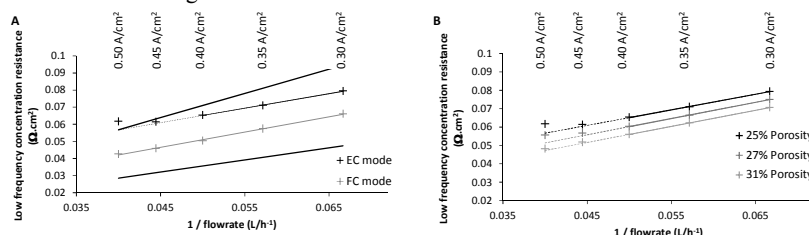
Figure 8. Measured low frequency concentration resistance during flow variations under current. A: Resistance measured in FC-mode and electrolysis cell mode for the cell with 25% porosity and B: Resistance measured during flow variations under current in electrolysis cell mode for cells with different porosity. The bold lines are the theoretical conversion resistance due to the different Nernst
20 potential based on a CSTR and a PFR model (½ of the SCTR model) respectively.

The conversion resistance at temperatures varying from 850ºC to 900ºC is shown in Figure 9. Again the bold lines represent the theoretical conversion resistances based on the CSTR or a PFR model. As can be seen, an increase in the resistance for the low frequency concentration arc increases with temperature.

25
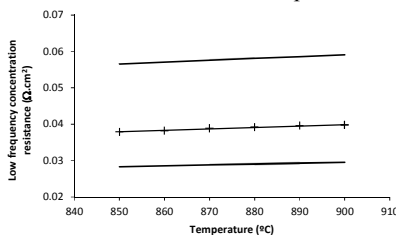
Figure 9. Conversion resistance for the cell with a porosity of 31% when characterised in 50% H_2O/50% H_2 at temperatures ranging from 850ºC to 900ºC. The bold lines are the theoretical conversion resistance due to the different Nernst potential based on a CSTR and a PFR model respectively.

30 ### Degradation

After testing the initial characterisation (iV and EIS at OCV) of the cells, durability in EC-mode was tested at 750, 800, or 850°C with 45% H_2O/ 45% CO_2/ 10% H_2 supplied to the Ni-YSZ electrode, oxygen supplied to the oxygen electrode, and a current density of -1.0 A/cm². The cell voltage evolution with time for Ni-

YSZ|YSZ|LSM-YSZ (Figure 10A) and Ni-YSZ|YSZ|CGO|LSCF-CGO cells (Figure 10B) operate at a reactant conversion of 60% is shown in Figure 10. From the experiments shown in Figure 10, degradation during electrolysis was observed for all tested cells, and a clear increase in degradation rate is observed when decreasing
5 the operation temperature for the Ni-YSZ|YSZ|LSM-YSZ cells. Similar, decreasing the temperature to 750ºC for the Ni-YSZ|YSZ|LSCF-CGO cells show an increase in degradation rate. Surprisingly, similar degradation rates were found at 800ºC and 850ºC for the Ni-YSZ|YSZ|CGO|LSCF-CGO cells. The Ni-YSZ|YSZ|CGO|LSCF-CGO shows an increased performance as compared to the Ni-YSZ|YSZ|LSM-YSZ
10 (lower initial cell voltage), whereas the degradation rates were comparable. When operating these SOECs at high current density (at or above $-1A/cm^2$) structural degradation occurs (evident by a change in the ohmic resistance, see Figure 11), which makes the degradation rates difficult to reproduce[67], thus, when looking at the cell voltage only, Figure 10 do not show any evident supporting an increased
15 durability (as reported in literature[59;60;62]) of the cell with an increased performance (Ni-YSZ|YSZ|CGO|LSCF-CGO).
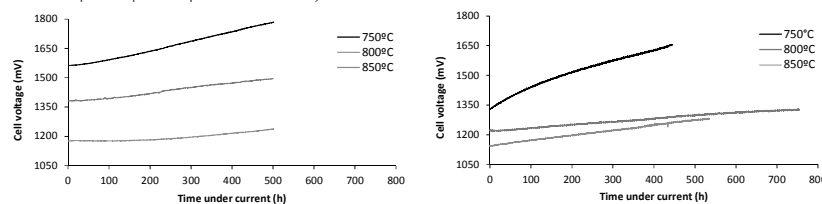
Figure 10. Cell voltage measured during co-electrolysis at 750ºC, 800ºC, and 850ºC at $-1.00A/cm^2$ and with 45% H_2O/ 45% CO_2/ 10% H_2 flown to the Ni-YSZ electrode. The reactant (H_2O+CO_2)
20 conversion was 60%.

The contribution to the degradation in overpotential from the different cell components was analysed by breaking down the impedance contribution measured during the durability test, Figure 11. From the data in Figure 11 it can be seen that the ohmic contribution to the degradation is higher for the Ni-YSZ|YSZ|LSM-YSZ
25 cells. A clear relation between the ohmic contribution to the degradation and the oxygen electrode with temperature occur for both cell types (increased degradation at lower temperature). On the other hand, the fuel electrode degradation seems independent of the operating temperature (beside the fuel electrode degradation observed for the Ni-YSZ|YSZ|CGO|LSCF-CGO cell operated at 850ºC, which is
30 surprisingly high) and is similar for all temperatures (for either Ni-YSZ|YSZ|LSM-YSZ cells or Ni-YSZ|YSZ|CGO|LSCF-CGO cells). The fuel electrode degradation for the Ni-YSZ|YSZ|CGO|LSCF-CGO cells are around 4 times higher than the fuel electrode degradation for the Ni-YSZ|YSZ|LSM-YSZ cells.

35

Ni-YSZ|YSZ|LSM-YSZ

Ni-YSZ|YSZ|CGO|LSCF-CGO
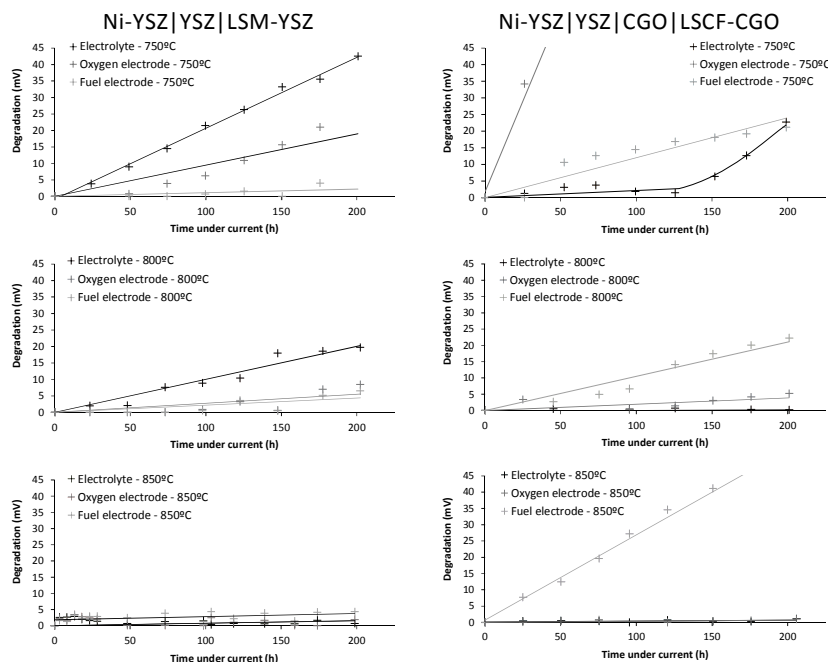
Figure 11. Breakdown of the degradation to the contribution from the fuel electrode, oxygen electrode and the electrolyte during the first 200 hours of operation of the cells shown in Figure 10.

The effect of the conversion degree on the degradation rate was investigated by performing two additional tests with YSZ|YSZ|CGO|LSCF-CGO cells; one
5 durability test was conducted at 800°C with 45% H_2O/45% CO_2/10% H_2 supplied to the Ni-YSZ electrode, and a current density of -1.0 A/cm^2 (identical to the test at 800°C, shown in Figure 10B), but with an increased flowrate as compared to the tests shown in Figure 10B, thus the reactant conversion was 30% (Figure 12A). Another test was carried out with 90% H_2O/10% H_2 supplied to the Ni-YSZ
10 electrode, and a current density of -1.0 A/cm^2, but with an initial reactant conversion of 30% and subsequently increased by steps of 10% conversion to reach a conversion degree of 90% (not shown). At both 30% and 60% reactant conversion (Figure 12A), the cell voltage during co-electrolysis show initially an increased degradation whereafter a linear long-term degradation was observed. From the
15 experiments shown in Figure 12A, it can be seen that increasing the reactant conversion from 30% to 60% do not influence the degradation rate. The test with increasing conversion degree showed that a reactant conversion degree of around 80 – 90% is necessary in order to observe an increase in degradation rate (not shown here).
20 Two additional tests were conducted to investigate the different degradation rates during steam and carbon monoxide electrolysis. When comparing the degradation rate during steam and carbon dioxide electrolysis (Figure 12B) it can be seen that a similar degradation rate is observed for the two tests, especially taking the reproducibility into account (if any difference is present a slightly higher
25 degradation is measured during electrolysis of carbon dioxide).
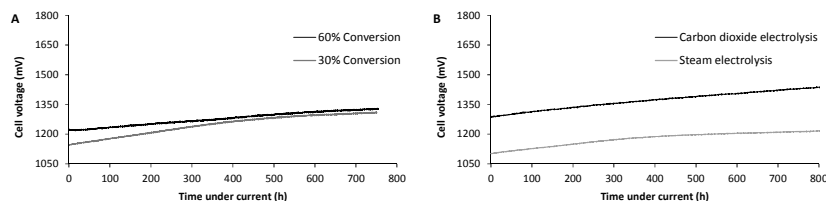
Figure 12. A: Cell voltage measured during co-electrolysis at 30% and 60% reactant (H_2O+CO_2) conversion with 45% H_2O/ 45% CO_2/ 10% H_2 flown to the Ni-YSZ electrode (the cell with 60% conversion is the same cell as shown in in Figure 10B). B: Cell voltage measured during either steam or carbon dioxide electrolysis at 60% reactant conversion with 90% H_2O/10% H_2 or 90% CO_2/ 10% CO flown to the Ni-YSZ electrode. All cells were operated at 800ºC, and a current density of -1.0A/cm^2.

Modelling the current and overpotential along the cell

A simple model to evaluate the effect of both porosity and reactant conversion on the Ni-YSZ TPB resistance was set up. Assuming a negligible in-plane voltage (which is normally below 1mV), the cell voltage is identical along the cell, whereas the resistance and overpotential (due to the Nernst potential as well as the relation between the steam partial pressure and Ni-YSZ TPB resistance) varies along the cell in the flow direction. Changing the reactant conversion will, although keeping the total current constant, change the current distribution along the cell (Figure 13A), which in turn alter the overpotential at the Ni-YSZ electrode. According to the relation between the resistances of the individual processes occurring the SOC and the current distribution, the overpotential at the Ni-TPB (which governs the degradation) can be found (Figure 13B) when neglecting diffusion limitations. Similar, the overpotential at the Ni-YSZ TPB with varying support structure can be found; here the difference is not due to the different conversion degree, but due to an altered current distribution and steam/hydrogen ration at the active nickel electrode due to diffusion Figure 13C. The overpotential (overvoltage) at the Ni-YSZ TPB increases when increasing the conversion degree due to the altered current distribution as well as the more reducing gas at the interface when increasing the reactant conversion. Thus, changing the reactant conversion may affect the degradation rate if, and only if degradation is observed in all cases. Similar increase, although much larger, in Ni-YSZ TPB over-potential, and thus increased degradation may be observed when decreasing the porosity of the support layer because the gas composition at the active electrode becomes increasingly reducing. Further, it is seen that decreasing the porosity the maximal Ni-YSZ TPB overpotential moves towards the inlet of the cell, thus if the degradation of the cell is correlated with the diffusion, an increased degradation at the inlet should be observed. Since both the reactant conversion and support structure affects the Ni-YSZ TPB resistance by changing the pO_2 at the active electrode, an interplay between the conversion degree and structural parameters do apply, and the diffusion limitations enhance the observed changes at the Ni-YSZ TPBs (Figure 13D). The results shown in Figure 13D are made based on a cell with a porosity of 28% (Ni-YSZ|YSZ|CGO|LSCF-CGO) in the support structure.
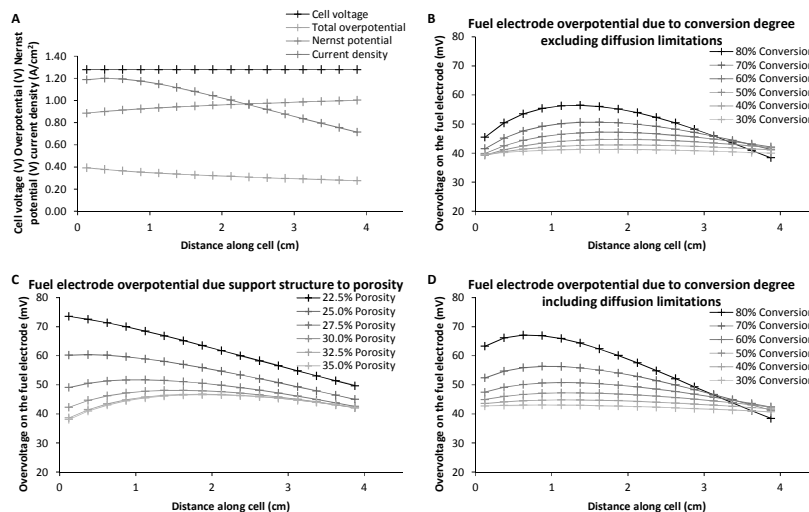
Figure 13. Calculated theoretical overpotential at the Ni-YSZ TPB along the cell. A: Variation of cell voltage, overpotential, Nernst potential and current density along the cell. B: Fuel electrode overpotential at various reactant conversion degrees neglecting diffusion limitations. C: Fuel electrode overpotential at various support structure porosities. D: Fuel electrode overpotential at various reactant conversion degrees taking diffusion through the support into account, based on a cell with a support structure porosity of 28%.

Discussion

Cell performance

Continuity of the i-V curves across OCV was observed for both H_2O/H_2 and CO_2/CO mixtures , showing that these Ni-YSZ SOCs can work as reversible SOCs in H_2O/H_2 and CO_2/CO mixtures as previous shown[18-20;68;92]. Each i-V curve yields two cell resistances, Area Specific cell Resistance (ASR) – one during oxidation of the reactants when applying positive current densities (operation in FC-mode, $ASR_{fuel\ cell}$) and the other during reduction of the reactants when applying negative current densities (operation in EC-mode, $ASR_{electrolysis}$). The observed ASR values in both H_2O/H_2 and CO_2/CO mixtures are lower for oxidation than for reduction, showing a marginally higher activity towards oxidation in comparison to reduction as previous been shown by several research groups [18-22]. Further, the ASR (both $ASR_{fuel\ cell}$ and $ASR_{electrolysis}$) were higher for CO_2/CO mixtures compared to the ASR values for H_2O/H_2 mixtures showing lower activity for CO oxidation/CO_2 reduction compared to H_2 oxidation/H_2O reduction in agreement with literature [18;19;68;91;92]. Figure 3, Figure 4 and Figure 5 shows that the electrode temperature drops when applying a negative current density (H_2O reduction, operated in EC-mode) and increases when applying a positive current density (H_2 oxidation, operated in FC-mode). During both oxidation and reduction, a temperature increase caused by polarisation heating of the cell will occur, and the polarisation heating will be identical during oxidation and reduction. As can be seen from Figure 3, the temperature increase during oxidation and decrease during reduction, and the change in temperature can therefore not solely be explained by polarisation heating. Besides the polarisation heating, the exothermic oxidation of H_2 and CO oxidation and the endothermic reduction of H_2O and CO_2 will inevitable result in a temperature increase during oxidation and a temperature decrease during reduction. Based on the

reaction enthalpy more heat will be produced/consumed when applying current in CO_2/CO mixtures which is in good agreement with Figure 3, Figure 4 and Figure 5. Further, at increasing cell voltage closer to or above the thermoneutral voltage, the temperature starts to increase. At 850ºC, the thermoneutral voltage for H_2O
5 electrolysis is 1.29 V. The current density where the temperature starts to increase was -0.55 A/cm^2 in the H_2O/H_2 mixture and -0.73A/cm^2 in the CO_2/CO mixture. Assuming an ASR of 0.21 Ω.cm^2 for reduction of H_2O, the current density where the cell voltage is equal to the thermoneutral voltage (1.29 V) is -1.57 A/cm^2 and the current density where the minimum temperature would be measured would thus be -
10 0.78 A/cm^2. The temperature profile show the expected trend, although the minimum temperature is observed at current densities slightly lower than expected, which may be because the ASR increases at high current densities due to conversion (Figure 3 and Figure 5), and because the added polarisation heating. This suggests that the temperature change is caused both by polarisation heating and the
15 exothermic/endothermic nature of the reactions.

The decreasing temperature will inevitably lead to an increased resistance of the thermal activated electrochemical reactions (Table 2) when operated in EC-mode as compared to when operated in FC-mode where heating will result in a lower ASR. The temperature profile measured during the DC characterisation may at least partly
20 explain the higher ASRs calculated for electrolysis versus the ASRs for fuel cell mode. The total resistances measured by the impedance measurements are in good agreement with the ARSs measured by DC characterisation (Figure 3, Figure 4 and Table 3).

The impedance spectra was analysed by breaking down the losses into an ohmic loss
25 and five polarisation losses ($R_{LSM – High}$, R_{TPB}, $R_{LSM – Low}$, $R_{Diffusion}$, and $R_{Conversion / low frequency concentration}$). Although the resistances for the individual arcs contributing to the Ni-YSZ electrode are larger in CO_2/CO mixtures, comparison of the impedance spectra and especially a DRT analysis for the two mixtures (Figure 4, Table 3), show that the spectra contain the same arcs. This suggests that the process in principle
30 consists of the same reaction type at the Ni-YSZ electrode irrespective of the gas mixture, and that the model may be applicable for both H_2O/H_2 and CO_2/CO mixtures. The ohmic resistance is comparable with the values obtained when establishing the model, whereas the resistances obtained for the electrochemical arcs ($R_{LSM – High}$, R_{TPB} and $R_{LSM – Low}$) are typically 10% lower [50]. The lower resistances in
35 the present may be a consequence of oxygen flown to the LSM-YSZ electrode (instead of air), and the higher steam concentration at the Ni-YSZ electrode, which increase the activity of these SOCs [50;82] (Figure 2).

The ohmic resistance show notable differences when applying current in both H_2O/H_2 and CO_2/CO mixtures (Figure 5). The most distinct temperature profile can
40 be seen during reduction of H_2O in H_2O/H_2 mixture, where the temperature reaches a minimum, whereafter it starts to increase again. The ohmic loss follows the exact same trend, clearly showing that the cell (and active electrodes) experiences a change in temperature. During oxidation in H_2O/H_2 the ohmic resistance decreased from 0.067 Ω.cm^2 to 0.064 Ω.cm^2, and increased to 0.072 Ω.cm^2 during reduction.
45 During oxidation in CO_2/CO the ohmic resistance decreased from 0.067 Ω.cm^2 to 0.061 Ω.cm^2, and increased to 0.073 Ω.cm^2 during reduction. A slightly larger temperature difference was measured during oxidation/reduction in the CO_2/CO mixture as compared to the H_2O/H_2 mixture, consistent with the larger change in ohmic resistance. The larger temperature change in the CO_2/CO mixture is

consistent with the higher reaction enthalpy for CO oxidation compared to H_2 oxidation (and for CO_2 reduction compared to H_2O reduction), and may observed some of the differences observed when comparing the reaction kinetics in H_2O/H_2 and CO_2/CO mixtures.

5 Based on both the AC and DC characterisation, the heat of reaction and polarisation heating during application of current definitely has an effect on the reaction kinetics, and may account for some of the differences, during operation in EC-mode as compared to FC-mode. The ohmic resistance may be used as measure of the actual electrode temperature, and show that the electrodes experience a significant higher

10 temperature change as measured by the thermocouple[25].

Due to the temperature changes, no reliable correlation/ discussion of the electrode kinetics can be made under current. On the other hand, diffusion and conversion which is close to independent of temperature changes (equation 4 and 8, and Figure 9) can be analysed as a function of applied current.

15 The calculated theoretical diffusion resistances compared to the experimentally found diffusion resistances are shown in Figure 6A. Because of the higher molar weight of CO_2/CO compared to H_2O/H_2 a higher $R_{Diffusion}$ is observed in CO_2/CO mixtures compared to H_2O/H_2 mixtures (Figure 4, Figure 5, and Figure 6). In general, the measured diffusion resistances are close to the theoretical values (Figure

20 6), although the experimental diffusion resistances are higher than the theoretical ones. Theoretically, the diffusion resistance is expected to be slightly higher in EC-mode compared to FC-mode for both H_2O/H_2 and CO_2/CO mixtures, in accordance with the experiments (Figure 6). For H_2O/H_2 mixtures, a gradual decrease occurs when decreasing the current in EC-mode and increasing current in FC mode, as

25 predicted theoretically. For CO_2/CO mixture, and increase at high FC-current is observed, also theoretically, this is predicted. A similar trend is found at OCV when varying either pH_2O or pCO_2 as shown in Figure 14.
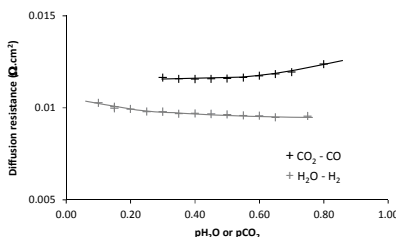
Figure 14. Measured (fitted) diffusion resistances in H_2O/H_2 and CO_2/CO mixtures as a function of
30 pH_2O or pCO_2.

Because the conversion resistance is only associated with the gas composition in the gas phase and not the molar masses the conversion resistance is expected to be identical for mixtures of H_2O/H_2 and CO_2/CO at "OCV", with a minimum in a 50% H_2O/ 50% H_2 mixture, and is expected to increase symmetrically around this

35 minimum with increasing/ decreasing H_2O/H_2 ratio (equation 4 and 8). Further, a slight increase with temperature as well as a linear relation with the inverse flow rate is expected. At OCV (Figure 8 Figure 15), as well as in FC-mode (Figure 8), the measured conversion / low frequency concentration resistance follows the theoretical predicted trends. As can be seen from Figure 5 and Figure 6B, the

40 observed low frequency concentration resistance is certainly not identical in H_2O/H_2

and CO_2/CO mixtures, and a significant higher low frequency concentration resistance is observed in CO_2/CO mixtures as compared to H_2O/H_2 mixture (Figure 6B). Figure 15 show the measured conversion resistance at OCV for the cell with a porosity of 25% compared to the measured low frequency concentration resistance
5 under current as a function of the average pH_2O along the cell. Further, also the theoretical conversion resistances based on the CSTR or a PFR model is shown by the bold lines in Figure 15. It is seen that the measured conversion resistance at OCV follows the trend predicted by the CSTR / PFR model, where the minimum conversion resistance is observed in a 50% H_2O/50% H_2 mixture, and increases
10 symmetrically around this minimum with increasing/ decreasing H_2O/H_2 ratio. In Figure 15, the observed conversion resistances lie between the values predicted by the two models, which makes sense when recalling the flow pattern for the set-up (Figure 1). Under current, the measured low frequency concentration resistance is highly asymmetric (Figure 5, Figure 6B, and Figure 15) with an increased low
15 frequency concentration resistance in EC-mode. This asymmetry is not due to the steam concentration, varying the inlet steam concentration from 45% to 55% show the exact same trend. Further, the asymmetry is higher in CO_2/CO mixtures as compared to H_2O/H_2 mixtures (Figure 5 and Figure 6B), and the asymmetry becomes more pronounced in CO_2/CO mixtures as compared to H_2O/H_2 mixtures
20 and increases with decreasing porosity (Figure 8). This show that the low frequency concentration resistance is affected by diffusion and may reflect the gas composition at the active Ni-YSZ electrode, and that a more precise description of the detailed nature of this arc remains to be modelled.
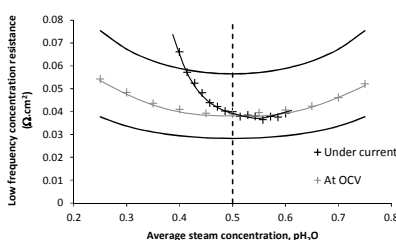
25 Figure 15. Comparison of the low frequency concentration resistance at 850ºC at OCV with varying the steam concentration with the low frequency concentration resistance measured under current (in 50% H_2O/50% H_2) as a function of the average steam concentration.

Even at OCV, the diffusion and the low frequency concentration resistance changes with support structure porosity, this means that the actual concentration at the active
30 fuel electrode varies with the structural parameters (Figure 7). Although the cells presented in this study were manufactured by sintering the half-cell at different temperatures, and thereby creating very different structural parameters for the active Ni-YSZ electrode, an increasing Ni-YSZ TPB resistance was observed with degreasing porosity (Figure 7B). This increased resistance may very well be due to
35 diffusion, changing the gas composition at the active Ni-YSZ TPB sites during the measurements, even at OCV. In general it is found that there is no pH_2 dependency for Ni-YSZ supported cells, whereas a significant dependency on pH_2O, pCO, and pCO_2 is found. Surprisingly, the Ni-YSZ TPB resistance dependency on apparent partial pressure of reactants and products, seem to correlate with the molar mass of
40 the species in question, and the observed dependency may thus be related to the diffusion, and thereby also the electrode structure. Therefore it may not be possible

to investigate electrode kinetics and make a general expression for "all" Ni-YSZ electrodes as this dependency will be dependent on the structural parameters of the specific cell.

The difference in performance for CO_2 electrolysis and H_2O electrolysis lies in both the Ni-YSZ TPB resistance, but also the slower diffusion, and thus higher low frequency concentration resistance.[27] When comparing H_2O electrolysis and co-electrolysis of H_2O and CO_2, almost identical Ni-YSZ TPB resistance and diffusion resistance is observed, whereas a slightly higher low frequency concentration resistance is observed during co-electrolysis.[27] Thus, the increased Ni-YSZ TPB resistance observed in CO_2/CO as compared to H_2O/H_2 mixtures may be associated with the diffusion through the support structure. This may be supported by studies on model electrodes (with no diffusion limitations) show much less difference between the performance in H_2O/H_2 and CO_2/CO mixtures[35;49;93;94].

When comparing co-electrolysis mechanism on fuel electrode supported cells and electrolyte supported cells[27;95-97] significant differences are found. For fuel electrode supported cells (for which diffusion through the support structure plays a role), a large difference between co-electrolysis and steam electrolysis performance is observed[27]. On the other hand, similar performance for co-electrolysis and steam electrolysis performance is observed for electrolyte supported cells[95-97] (where no diffusion restrictions occurs). These differences may be explained by diffusion, affecting both the Ni-YSZ TPB and the low frequency concentration resistance in a Ni-YSZ supported cell. Probably, a diffusion limiting current density is reached in the active Ni-YSZ layer next to the electrolyte, i.e. pH_2O and pCO_2, respectively, approaches zero and then the Ni-YSZ support starts to become electrochemically active, but it has a much higher polarisation resistance due to its coarse structure, and this high resistance results in a very long time constant (a large low frequency arc). A modelling of this will require a very detailed 3D, which is not available to us.

The large effect of the structural parameters indicates that electrolyte supported or oxygen electrode supported cells may be preferable as electrolysis cells as these will minimise the diffusion limitations and decrease the Ni-YSZ TPB resistance (caused by diffusion limitations). Similar, pressurised operation may significantly increase the performance of these cells, again by decreasing the diffusion limitations and Ni-YSZ TPB resistance.

Cell degradation

A long-term degradation for the SOCs during electrolysis operation was observed for all tests by the course of the cell voltage (Figure 10) and the increase in impedance (Figure 11). These cells show degradation in both the serial resistance as well as the polarisation resistances. From the cell voltages shown in Figure 10 it can be seen that lowering the operation temperature increases the degradation rate of the cells. There is a clear correlation between the operation temperature and the degradation rate for the oxygen electrode (and electrolyte) whereas the degradation for the fuel electrode does not seem to depend on the operation temperature. The degradation at the oxygen electrode (and electrolyte) is therefore most likely related to the overpotential as previously discussed[14;61;63]. On the other hand, the degradation at the fuel electrode cannot be correlated to the temperature. It has previously been suggested that the observed degradation is caused by metallic inter-diffusion of Zr formed by reduction of YSZ at low oxygen partial pressures (a critical pO_2 of $3.2\times10^{-29\pm3}$ bar at 850°C[98]). Such low oxygen partial pressures imply

an overpotential at the Ni-YSZ TPB of several hundred mV[98]. It is difficult to imagine such low oxygen partial pressures/ high overpotential at the Ni-YSZ TPB (Figure 13) unless significant diffusion limitations occur. The Ni-YSZ degradation is higher for the Ni-YSZ|YSZ|CGO|LSCF-CGO cells as compared to the Ni-
5 YSZ|YSZ|LSM-YSZ cells. Although an increased polarisation at the oxygen electrode do smoothen the current distribution along the cell for the Ni-YSZ|YSZ|LSM-YSZ cells, this is far from enough to explain the difference observed. On the other hand, the support structure porosity for the Ni-YSZ|YSZ|LSM-YSZ cells (34%) is higher than for the Ni-YSZ|YSZ|CGO|LSCF-
10 CGO (28%). Based on the discussion above, such a decrease in porosity will inevitably create a decreased pO_2 at the interface due to diffusion limitations (Figure 13), and the porosity may be critical for the observed degradation. This is consistent with the carbon formation observed in the Ni-YSZ electrode close to the YSZ electrolyte in cells operated far outside the carbon deposition regime[99;100], indicating
15 a very reducing atmosphere.

Careful analysis of the degradation of these cells have shown that degradation in the Ni-YSZ electrode is found close to the inlet of the cell[101]. The increased diffusion limitations, will, due to the lower steam concentration at the interface move the maximal overpotential at the Ni-YSZ electrode closer to the inlet (Figure 13), thus
20 supporting that diffusion limitation may play a significant role for the degradation of these cells. Due to changes in diffusion, similar increased degradation may be found by increasing the reactant conversion (Figure 13) as well an increased degradation may be observed during CO_2 electrolysis (as compared to steam electrolysis). Within the experientially uncertainties, no evidence for an increased degradation was
25 observed when increasing the conversion degree from 30% to 60% (Figure 12A), nor an influence of CO_2 electrolysis as compared to steam electrolysis (Figure 12Figure 12B) was found. A reactant conversion of at least 80% was necessary in order to observe an increase in degradation rates. The effect of support structure and the effect of reactant conversion are related, and without significant diffusion
30 limitations, the conversion degree has only a minor effect on the degradation rate. In this study we did not find any clear correlation between the long term degradation and the conversion degree, whereas in literature there is a huge disagreement, whether the conversion degree influences the degradation rate of the cells.[14] Beside the obvious effect of impurities in the gas phase (and in raw materials) which will be
35 affected by the steam partial pressure (the decreasing steam partial pressure due to the conversion will cause an increased deposition of the steam bore impurities in the Ni-YSZ cathode), and that the impurity level may be higher in CO_2/CO mixtures as compared to H_2O/H_2, the presence of impurities may explain the increased degradation with increased reactant conversion as well as in carbon dioxide
40 sometimes observed in literature, but for CO_2 the degradation rate should not be dependent on the degree of conversion as long as there is no significant diffusion limitation. That similar degradation rates were observed in steam and carbon dioxide mixtures and at 30% or 60% reactant conversion in the present study may be due to the fact that the inlet gases were cleaned to eliminate impurity related degradation.
45 Adsorption of impurities[18;66;102] as well as structural changes[101;103;104] during durability tests have shown to alter the measured low frequency concentration resistance. Assuming that the low frequency concentration resistance is in fact dependant on the electrode structure, such changes may be explained since the active Ni-YSZ TPB alters in these cases. For example if degradation occurs at the

electrode|electrolyte interface, the active Ni-YSZ TPBs move away from the interface, changing the diffusion distance.

When comparing the tests with different reduction temperature (Figure 12A compared to Figure 12B), it can be seen that a slightly lower degradation rate is found for the cells reduced at 1000ºC (850ºC for the two cells shown in Figure 12A, as compared to 1000ºC for the two cells shown in Figure 12B). The decreased degradation rate for the cells reduced at a higher temperature may be due to the increased mechanical strength induced by the higher reduction temperature[105].

Conclusion

Ni-YSZ electrode supported Solid Oxide Cell (SOC) was operated in both fuel cell mode (FC-mode) and electrolysis cell mode (EC-mode) in mixtures of H_2O/H_2, CO_2/CO, $H_2O/H_2O/CO_2/CO$ at 750ºC, 800ºC and 850ºC. Polarisation (i-V) characterisation show that the kinetics for reduction of H_2O and CO_2 is slightly slower compared to oxidation of H_2 and CO. The slower kinetic for reduction was found to be partly related to the polarisation heating and the entropy change. Due to the exothermic reaction in FC-mode and endothermic reaction in EC-mode, both the ohmic resistance as well as the electrochemical electrode resistances are higher in EC-mode as compared to FC-mode. The measured diffusion resistance is slightly larger in EC-mode as compared to FC-mode whereas the low frequency concentration resistance is significant higher in EC-mode at high current densities, probably related to diffusion limiting current densities. Both the increased diffusion resistance and the asymmetric low frequency concentration resistance result in an increased Area Specific Resistance (decreased activity) in EC-mode. The temperature profile shows a decrease in temperature when going from FC-mode to EC-mode due to the exothermic nature of the oxidation and endothermic nature of the reduction. The lower performance in EC-mode compared to FC-mode close to open circuit voltage (OCV) may therefore be explained by the temperature changes caused by the reactions. At higher current densities the increase caused by diffusion limitations become more pronounced and may explain the apparent fuel starvation normally observed at lower conversion degrees in EC-mode as compared to FC-mode. Changing the porosity of the support structure show a change the Ni-YSZ TPB resistance and a significant change in the low frequency concentration (partial pressure) related resistance when applying high current densities. The observed increased polarisation in EC-mode at decreasing porosity shows that diffusion limitations cannot be neglected for support structures with porosity below 30% (with a support thickness of 300μm). These diffusion limitations through the support and active electrode structure create an increased reducing atmosphere at the interface which may be related to the degradation of the cells.

Acknowledgement

References

1 A. O. Isenberg *Solid State Ionics* 1981, *3-4,* 431.
2 W. Donitz, E. Erdle *Int. J. Hydrogen Energy* 1985, *10,* 291.
3 W. Dönitz, E. Erdle, R. Schaumm, R. Streicher *Adv. Hydrogen Energy* 1988, *6,* 65.
4 Dönitz, W.; Erdle, E.; Streicher, R. High Temperature Electrochemical Technology For Hydrogen Production and Power Generation. In *Electrochemical hydrogen technologies: Electrochemical production and combustion of hydrogen*; Wendt, H. Elsevier: Amsterdam, The Netherlands, 1990.
5 W. Dönitz, G. Dietrich, E. Erdle, R. Streicher *Int. J. Hydrogen Energy* 1988, *13,* 283.
6 W. Doenitz, R. Schmidberger *Int. J. Hydrogen Energy* 1982, *7,* 321.
7 K. H. Quandt, R. Streicher *Int. J. Hydrogen Energy* 1986, *11,* 309.
8 H. S. Spacil, C. S. Tedmon *J. Electrochem. Soc.* 1969, *116,* 1618.
9 E. Erdle, W. Donitz, R. Schamm, A. Koch *Int. J. Hydrogen Energy* 1992, *17,* 817.
10 Elikan, L.; Morris, J. P.; Wu, C. K. *Development of a Solid Electrolyte Carbon Dioxide and Water Reduction System for Oxygen recovery, NASA Report CR-2014;* Report for NASA Research Center, 1972.
11 Isenberg, A. O.; Cusick, R. J. *Carbon Dioxide Electrolysis with Solid Oxide Electrolyte Cells for Oxygen Recovery in Life Support System,* 18th Intersociety Conference on Environmental Systems pp. Paper 881040, San Franscisco, California, USA, 1989.
12 Isenberg, A. O. *Three-man Solid Electrolyte Carbon Dioxide Electrolysis Breadboard, NASA Report CR-185612;* Report for NASA Research Center, 1989.
13 K. R. Sridhar *J. Br. Interplanet. Soc.* 1996, *49,* 435.
14 S. D. Ebbesen, S. H. Jensen, A. Hauch, M. Mogensen *Chem. Rev.* 2014, *114,* 10697.
15 A. Hagen, R. Barfod, P. V. Hendriksen, Y. L. Liu, S. Ramousse *J. Electrochem. Soc.* 2006, *153,* A1165.
16 Hauch, A. *Solid Oxide Electrolysis Cells - Performance and Durability*, PhD Thesis, Risø National Laboratory, Risø, Roskilde, Denmark, **2007**
17 S. H. Jensen, A. Hauch, P. V. Hendriksen, M. Mogensen, N. Bonanos, T. Jacobsen *J. Electrochem. Soc.* 2007, *154,* B1325.
18 S. D. Ebbesen, M. Mogensen *J. Power Sources* 2009, *193,* 349.
19 S. D. Ebbesen, C. Graves, M. Mogensen *Int. J. Green Energy* 2009, *6,* 646.
20 A. Hauch, S. H. Jensen, S. Ramousse, M. Mogensen *J. Electrochem. Soc.* 2006, *153,* A1741.
21 O. A. Marina, L. R. Pederson, M. C. Williams, G. W. Coffey, K. D. Meinhardt, C. D. Nguyen, E. C. Thomsen *J. Electrochem. Soc.* 2007, *154,* B452.
22 Mogensen, M. *Electrode kinetics of SOFC anodes and cathodes,* Proceedings of the 14th Risø international symposium on materials science, High temperature electrochemical behaviour of fast ion and mixed conductors, Risø, Roskilde, Denmark, September 6-9, 1993; pp. 117, Poulsen, F. W., Bentzen, J. J., Jacobsen, T., Skou, E., Østergård, M. J. L. Risø National Laboratory: Risø, Roskilde, Denmark, 1993.
23 G. B. Jung, J. Y. Chen, C. Y. Lin, S. Y. Sun *Int. J. Hydrogen Energy* 2012, *37,* 15801.
24 M. Ni, M. K. H. Leung, D. C. Leung *J. Power Sources* 2006, *163,* 460.
25 S. D. Ebbesen, M. Mogensen *ECS Trans.* 2013, *50,* 167.
26 J. C. Njodzefon, D. Klotz, A. Kromp, A. Weber, E. Ivers-Tiffée *J.*

Electrochem. Soc. 2013, ***160,*** F313.

27   S. D. Ebbesen, R. Knibbe, M. Mogensen *J. Electrochem. Soc.* 2012, ***159,*** F482.

28   T. H. Etsell, S. N. Flengas *J. Electrochem. Soc.* 1971, ***118,*** 1890.

5   29   C. J. Wen, D. M. Mason *J. Appl. Electrochem.* 1978, ***8,*** 81.

30   R. Suwanwarangkul, E. Croiset, M. W. Fowler, P. L. Douglas, E. Entchev, M. A. Douglas *J. Power Sources* 2003, ***122,*** 9.

31   M. Ni *Chem. Eng. J.* 2010, ***164,*** 246.

32   M. Ni *Int. J. Hydrogen Energy* 2009, ***34,*** 7795.

10   33   M. Ni *Int. J. Hydrogen Energy* 2012, ***37,*** 6389.

34   Y. Matsuzaki, I. Yasuda *J. Electrochem. Soc.* 2000, ***147,*** 1630.

35   A. Utz, K. V. Hansen, K. Norrman, E. Ivers-Tiffée, M. Mogensen *Solid State Ionics* 2011, ***183,*** 60.

36   M. S. Schmidt, K. V. Hansen, K. Norrman, M. Mogensen *Solid State Ionics*

15   2009, ***180,*** 431.

37   A. Leonide, S. Hansmann, A. Weber, E. Ivers-Tiffée *J. Power Sources* 2011, ***196,*** 7343.

38   A. Bieberle, L. P. Meier, L. J. Gauckler *J. Electrochem. Soc.* 2001, ***148,*** A646.

20   39   Mogensen, M.; Sunde, S.; Primdahl, S. *SOFC anode kinetics,* Proceedings of the 17th Risø International Symposium on Materials Science: High Temperature Electrochemistry: Ceramisc and Metals, Denmark, Risø, Roskilde, Denmark, September 2-9, 1996; pp. 77, Poulsen, F. W., Bonanos, N., Linderoth, S. Risø National Laboratory: Risø, Roskilde, Denmark, 1996.

25   40   Mizusaki, J.; Yamamura, T.; Mori, K.; Tagawa, H.; Hirano, K.; Ehara, S.; Takagi, T.; Hishinuma, M.; Sasaki, H.; Sogi, T.; Nakamura, Y.; Hashimoto, K. *Kinetic Studies on Ni/YSZ Anodes Reaction of SOFC in H2-H2O Atmospheres By the use of Nickel Pattern Electrodes,* Proceedings of the 17th Risø International Symposium on Materials Science: High Temperature

30   Electrochemistry: Ceramisc and Metals, Denmark, Risø, Roskilde, Denmark, September 2-9, 1996; pp. 363, Poulsen, F. W., Bonanos, N., Linderoth, S. Risø National Laboratory: Risø, Roskilde, Denmark, 1996.

41   M. Mogensen, K. V. Jensen, M. J. Jørgensen, S. Primdahl *Solid State Ionics* 2002, ***150,*** 123.

35   42   M. Mogensen, J. Høgh, K. V. Hansen, T. Jacobsen *ECS Trans.* 2007, ***7,*** 1329.

43   S. P. Jiang, S. P. S. Badwal *Solid State Ionics* 1999, ***123,*** 209.

44   J. Mizusaki, H. Tagawa, T. Saito, K. Kamitani, T. Yamamura, K. Hirano, S. Ehara, T. Takagi, T. Hikita, M. Ippommatsu, S. Nakagawa, K. Hashimoto *J. Electrochem. Soc.* 1994, ***141,*** 2129.

40   45   M. Ni, M. K. H. Leung, D. Y. C. Leung *Int. J. Hydrogen Energy* 2007, ***32,*** 2305.

46   S. Primdahl, M. Mogensen *J. Electrochem. Soc.* 1997, ***144,*** 3409.

47   S. P. Jiang, S. P. S. Badwal *J. Electrochem. Soc.* 1997, ***144,*** 3777.

48   M. Brown, S. Primdahl, M. Mogensen *J. Electrochem. Soc.* 2000, ***147,*** 475.

45   49   A. Utz, A. Leonide, A. Weber, E. Ivers-Tiffée *J. Power Sources* 2011, ***196,*** 7217.

50   R. Barfod, M. Mogensen, T. Klemenso, A. Hagen, Y. L. Liu, P. V. Hendriksen *J. Electrochem. Soc.* 2007, ***154,*** B371.

51   V. Sonn, A. Leonide, E. Ivers-Tiffée *J. Electrochem. Soc.* 2008, ***155,*** B675.

50   52   Juhl, M.; Primdahl, S.; Mogensen, M. *Characterisation of Composite SOFC Cathodes by Impedance Spectroscopy,* Proceedings of the 17th Risø International Symposium on Materials Science: High Temperature Electrochemistry: Ceramisc and Metals, Denmark, Risø, Roskilde, Denmark, September 2-9, 1996; pp. 295, Poulsen, F. W., Bonanos, N., Linderoth, S.

Risø National Laboratory: Risø, Roskilde, Denmark, 1996.

53   M. J. Jørgensen, M. Mogensen *J. Electrochem. Soc.* 2001, *148,* A433.

54   C. Peters, A. Weber, E. Ivers-Tiffée *J. Electrochem. Soc.* 2008, *155,* B730.

55   O'Brien, J. E.; Housley, G. K.; Milobar, D. G.; Petigny, N. *Performance of Single Electrode-Supported Cells Operating in the Electrolysis Mode,* Proceedings of the ASME 2009 International Mechanical Engineering Congress and Exposition, IMECE2009, Lake Buena Vista, Florida, USA, November 13–19, 2009; pp. 617, ASME: 2009.

56   T. Matsui, R. Kishida, J. Y. Kim, H. Muroyama, K. Eguchi *J. Electrochem. Soc.* 2010, *157,* B776.

57   Mansuy, A.; Mougin, J.; Petitjean, M.; Mauvy, F. *Durability studies of Solid Oxide Electrolysis Cells (SOEC),* Proceedings of the 10th European SOFC forum, Luzern, Switzerland, July 26-29, 2012; pp. B0704, European Fuel Cell Forum AG: Luzern, Switzerland, 2012.

58   Tang, E.; Wood, T.; Benhaddad, S.; Brown, C.; He, H.; Nelson, J.; Grande, O.; Nuttal, B.; Richards, M.; Petri, R. *Advanced Materials for RSOFC Dual Operation with Low Degradation;* Report for United States Department of Energy, 2012.

59   Guan, J.; Minh, N.; Ramamurthi, B.; Ruud, J.; Hong, J.-K.; Riley, P.; Weng, D. *High Performance Flexible Reversible Solid Oxide Fuel Cell, Final Technical Report;* Report for United States Department of Energy, 2006.

60   N. Q. Minh *ECS Trans.* 2011, *35,* 2897.

61   K. Chen, N. Ai, S. P. Jiang *J. Electrochem. Soc.* 2010, *157,* P89.

62   P. Hjalmarsson, X. Sun, Y.-L. Liu, M. Chen *J. Power Sources* 2013, *223,* 349.

63   A. Momma, T. Kato, Y. Kaga, S. Nagata *J. Ceram. Soc. Jpn.* 1997, *105,* 369.

64   Larsen, P. H.; Bagger, C.; Linderoth, S.; Mogensen, M.; Primdahl, S.; Jørgensen, M. J.; Hendriksen, P. V.; Kindl, B.; Bonanos, N.; Poulsen, F. W.; Maegaard, K. A. Proceedings of Solid Oxide Fuel Cell VII (SOFC VII) pp. 28, Yokokawa, H., Singhal, S. C. Electrochem.Soc.: Pennington, NJ, 2001.

65   M. J. Jørgensen, M. Mogensen *J. Electrochem. Soc.* 2001, *148,* A433.

66   S. D. Ebbesen, C. Graves, A. Hauch, S. H. Jensen, M. Mogensen *J. Electrochem. Soc.* 2010, *157,* B1419.

67   Ebbesen, S. D. Durability of Solid Oxide Electrolysis Cells. In *Green Natural Gas, Energy Technology Development and Demonstration Programme (EUDP) under the Danish Energy Agency*2014.

68   S. D. Ebbesen, M. Mogensen *Electrochem. Solid-State Lett.* 2010, *13,* B106.

69   A. Hauch, M. Mogensen *Solid State Ionics* 2010, *181,* 745.

70   Ebbesen, S. D.; Mogensen, M. Method and System for Purification of Gas Streams for Solid Oxide Cells. EP2362475A1, 2010.

71   Ebbesen, S. D.; Mogensen, M. Method and System for Purification of Gas Streams for Solid Oxide Cells. EP2537203 A1, 2011.

72   Birkl, C. *Eects of anode sintering temperature on microstructure and performance of multilayer tape cast SOFC*, MsC Thesis, DTU Energy Conversion, Risø Campus, Technical University of Denmark, Roskilde, Denmark, **2012**

73   Hauch, A.; Birkl, C.; Brodersen, K.; Jørgensen, P. S. *Multilayer tape cast SOFC - Effect of anode sintering temperature,* Proceedings of the 10th European SOFC forum, Luzern, Switzerland, July 26-29, 2012; pp. A1007, European Fuel Cell Forum AG: Luzern, Switzerland, 2012.

74   S. Primdahl, M. Mogensen *J. Electrochem. Soc.* 1999, *146,* 2827.

75   J. R. Izzo, A. S. Joshi, K. N. Grew, W. K. S. Chiu, A. Tkachuk, S. H. Wang, W. Yun *J. Electrochem. Soc.* 2008, *155,* B504.

76   R. E. Williford, L. A. Chick, G. D. Maupin, S. P. Simner, J. W. Stevenson *J.*

Electrochem. Soc. 2003, **150,** A1067.

77 H. Iwai, N. Shikazono, T. Matsui, H. Teshima, M. Kishimoto, R. Kishida, D. Hayashi, K. Matsuzaki, D. Kanno, M. Saito, H. Muroyama, K. Eguchi, N. Kasagi, H. Yoshida *J. Power Sources* 2010, **195,** 955.

78 J. R. Wilson, J. S. Cronin, S. A. Barnett *Scripta Materialia* 2011, **65,** 67.

79 Jørgensen, P. S. *Quantitative Data Analysis Methods for 3D Microstructure Characterization of Solid Oxide Cells*, PhD Thesis, Technical University of Denmark, Kongens Lyngby, Denmark, **2010**

80 S. Primdahl, M. Mogensen *J. Electrochem. Soc.* 1998, **145,** 2431.

81 S. H. Jensen, A. Hauch, P. V. Hendriksen, M. Mogensen *J. Electrochem. Soc.* 2009, **156,** B757.

82 A. Hagen, M. Menon, R. Barfod, P. V. Hendriksen, S. Ramousse, P. H. Larsen *Fuel Cells* 2006, **6,** 146.

83 J. Nielsen, J. Hjelm *Electrochim. Acta* 2014, **115,** 31.

84 Primdahl, S.; Hendriksen, P. V.; Larsen, P. H.; Kindl, B.; Mogensen, M. *Evaluation of SOFC test data,* Proceedings of Solid Oxide Fuel Cell VII (SOFC VII), Tsukuba, Japan, June 5-8, 2001; pp. 932, Singhal, S. C., Yokokawa, H. Electrochemical Society, Inc.: Pennington, New Jersey, USA, 2001.

85 S. P. S. Badwal *Solid State Ionics* 1992, **52,** 23.

86 E. P. Murray, T. Tsai, S. A. Barnett *Solid State Ionics* 1998, **110,** 235.

87 Juhl, M.; Primdahl, S.; Mogensen, M. *CHARACTERISATION OF COMPOSITE SOFC CATHODES BY IMPEDANCE SPECTROSCOPY,* Proceedings of the 17th Risø International Symposium on Materials Science: High Temperature Electrochemistry: Ceramisc and Metals, Denmark pp. 295, Poulsen, F. W., Bonanos, N., Linderoth, S.Roskilde, Denmark, 1996.

88 A. Leonide, V. Sonn, A. Weber, E. Ivers-Tiffée *J. Electrochem. Soc.* 2008, **155,** B36.

89 E. Siebert, A. Hammouche, M. Kleitz *Electrochim. Acta* 1995, **40,** 1741.

90 Christiansen, N.; Hansen, J. B.; Holm-Larsen, H.; Linderoth, S.; Larsen, P. H.; Hendriksen, P. V.; Hagen, A. *Solid Oxide Fuel Cell Development at Topsoe Fuel Cell A/S and Risø National Laboratory,* Proceedings of Risø International Energy Conference, Energy solutions for sustainable development., Risø, Roskilde, Denmark, May 22-24, 2007; pp. 357, Petersen, S. L., Larsen, H. Risø National Laboratory: Risø, Roskilde, Denmark, 2007.

91 P. Holtappels, L. G. J. de Haart, U. Stimming, I. C. Vinke, M. Mogensen *J. Appl. Electrochem.* 1999, **29,** 561.

92 S. H. Jensen, P. H. Larsen, M. Mogensen *Int. J. Hydrogen Energy* 2007, **32,** 3253.

93 A. Utz, H. Störmer, A. Leonide, A. Weber, E. Ivers-Tiffée *J. Electrochem. Soc.* 2010, **157,** B920.

94 A. Ehn, J. Høgh, M. Graczyk, K. Norrman, L. Montelius, M. Linne, M. Mogensen *J. Electrochem. Soc.* 2010, **157,** B1588.

95 C. M. Stoots, J. E. O'Brien, J. S. Herring, J. J. Hartvigsen *J. Fuel Cell Sci. Technol.* 2009, **6,** 011014.

96 C. Stoots, J. O'Brien, J. Hartvigsen *Int. J. Hydrogen Energy* 2009, **34,** 4208.

97 C. M. Stoots, J. E. O'Brien, K. G. Condie, J. J. Hartvigsen *Int. J. Hydrogen Energy* 2010, **35,** 4861.

98 M. Chen, Y. L. Liu, J. J. Bentzen, W. Zhang, X. Sun, A. Hauch, Y. Tao, J. R. Bowen, P. V. Hendriksen *J. Electrochem. Soc.* 2013, **160,** F883.

99 Y. Tao, S. D. Ebbesen, M. Mogensen *J. Electrochem. Soc.* 2014, **161,** F337.

100 Y. Tao, S. D. Ebbesen, W. Zhang, M. B. Mogensen *ChemCatChem* 2014, **6,** 1220.

101 X. Sun, M. Chen, Y. L. Liu, P. V. Hendriksen, M. Mogensen *ECS Trans.*

2013, **57,** 3229.

102 A. Hauch, A. Hagen, J. Hjelm, T. Ramos *J. Electrochem. Soc.* 2014, **161,** F734.

103 Tao, Y. *Durability of the Solid Oxide Cells for Co-Electrolysis of Steam and Carbon Dioxide under High Current Densities*, PhD Thesis, DTU Energy Conversion, Risø Campus, Technical University of Denmark, Roskilde, Denmark, **2014**

104 P. Hjalmarsson, X. Sun, Y. L. Liu, M. Chen *J. Power Sources* 2014, **262,** 316.

105 A. Faes, H. L. Frandsen, M. Pihlatie, D. R. Goldstein *J. Fuel Cell Sci. Technol.* 2010, **7,** 051011-1.